Thermodynamic re-modeling of the Yb-Sb system aided by first-principles calculations

Jorge Paz Soldan Palma*[1], XiaoYu Chong[1,2], Yi Wang[1], Shun-Li Shang[1] and Zi-Kui Liu[1]

[1]Department of Materials Science and Engineering, The Pennsylvania State University, University Park, PA 16802, USA

[2]Kunming University of Science and Technology, Kunming, 650093, China

* Corresponding author: jfp21@psu.edu

Abstract

The thermodynamic description of the Yb-Sb binary system is developed by means of the CALculations of PHAse Diagrams (CALPHAD) method by combining experimental data and first-principles calculations based on Density Functional Theory (DFT) in the literature. Two pseudopotentials for Yb were compared in the study: one with all 14 *f*-electrons frozen in the core and the other with 13 *f*-electrons frozen in the core. It was observed that the pseudopotential with 13 *f*-electrons frozen in the core presented no imaginary modes in the phonon calculations for cubic YbSb and was subsequently applied to predict the aforementioned structure's temperature dependent thermodynamic properties by the DFT-based quasiharmonic phonon calculations. The current thermodynamic database includes all five phases that were considered in preceding modeling studies in addition to the $Yb_{16}Sb_{11}$ compound, which was not considered previously. The study also rectifies the plausible misconception of the high temperature transformation of the Yb_5Sb_3 compound. The associate solution model is used to describe the short-range ordering behavior in the liquid phase. The resulting thermodynamic model showed good agreement with literature observations.

Keywords: Yb-Sb system; CALPHAD; Phonon; First-principles calculations; Thermoelectrics

1 Introduction

The Yb-Sb system has multiple compounds that have electronic, magnetic, and superconducting properties of interest to the scientific community [1–3]. This binary system plays a large role in the thermoelectric community where the Yb-Sb-containing compounds such as $Yb_{14}MnSb_{11}$, $Ca_{1-x}Yb_XZn_2Sb_2$, $YbSb_2Te_4$, and Yb_xCoSb_3 [4–11] have shown remarkable figure of merit, zT, values at different temperature ranges and are considered candidates for future thermoelectric generators [12].

A thermodynamic model of the Yb-Sb system, based on the studies by Abulkhaev et al. [13] and Pratt et al. [14], was developed alongside the Ho-Sb system [15]. However, the model contains inconsistencies with experimental data in the literature such as the absence of the $Yb_{16}Sb_{11}$ compound [16,17] and the inclusion of the hydrogen stabilized orthorhombic $Yb_5Sb_3H_x$ compound [3,18] as binary phase. The model also described the parameterized Gibbs energy function of the intermetallic compounds with the Neumann-Kopp approach due to the lack of temperature dependent thermochemical data in the literature at that time, an issue addressed in Chong et al.'s work [19]. Furthermore, the model doesn't take into consideration the effect of gas phase in the system, which has been observed to play a large role in the thermodynamic stability of Yb-rich compounds at high temperatures [20,21].

The present work aims to re-model the Yb-Sb system based on the latest thermochemical and phase equilibria data, see details in Section 2, alongside first-principles calculations based on density functional theory (DFT) [19,22,23]. The ultimate goal of the present work is to develop a multicomponent database that will help describe the interface stability of $Yb_{14}MnSb_{11}$ when contacted with metal hot shoes [20,24] for high temperature thermoelectric generator applications.

2 Literature Review

2.1 Phase equilibria data

Bodnar et al. [25] identified six intermetallic compounds by X-ray diffraction analysis (XRD) (Yb_5Sb_2, Yb_5Sb_4, Yb_5Sb_3, Yb_4Sb_3, YbSb, $YbSb_2$) and measured the melting points through an optical pyrometer. The study determined that Yb rich portions were in equilibrium with the gas phase and Yb_4Sb_3 melted congruently at 1540 ºC. Steinfink et al. [26] later showed through XRD patterns that the Yb_5Sb_4 compounds identified by Bodnar et al. [25] actually had the $Yb_{11}Sb_{10}$ stoichiometry with the $Ho_{11}Ge_{10}$ crystal structure and magnetic susceptibility measurements determined Yb to be divalent in this state. Abulkhaev et al.[13] conducted a study of the whole composition range based on differential thermal analysis (DTA), XRD and microstructural analysis. According to the DTA portion of the study , the Yb_4Sb_3 compound melts congruently at 1680ºC but did not comment on observing the gas phase. All other compounds were determined to melt non-congruently at lower temperatures. A transformation of the Yb_5Sb_3 intermetallic compound at 1280 ºC was also observed , from a lower temperature orthorhombic structure to a high temperature hexagonal structure. The XRD analysis confirmed the existence of $YbSb_2$, Yb_4Sb_3, $Yb_{11}Sb_{10}$, YbSb, and both α- and β- Yb_5Sb_3. The temperatures and compositions of the invariant reactions and liquidus measured by Abulkhaev et al. [13] will be incorporated and given priority over Bodnar et al.'s [25] measurements in the present work because of its more correct identification of the intermetallic phases.

Escamilla et al.[18] later discovered that the transition between α-Yb_5Sb_3 and β-Yb_5Sb_3 was an artifact of hydrogen contamination. The study demonstrated it by exposing the orthorhombic Yb_5Sb_3 to elevated temperatures in a dynamic vacuum, leading to the sublimation of hydrogen. This resulted in the formation

of only the hexagonal Yb_5Sb_3 phase and ~5% phase fraction of the $Yb_{16}Sb_{11}$ Zintl compound, which was discovered in a separate study by Escamilla et al. [16]. The claim of the orthorhombic structure being hydrogen stabilized is further supported by the work of Lu et al. [3], where the methods applied to form both hexagonal and orthorhombic Yb_5Sb_3 structure were based on Escamilla et al.'s [18,27] synthesis method. The aforementioned studies determined the existence of $Yb_{16}Sb_{11,}$ which was not observed in the study by Abulkhaev et al.[13], and removed the α-Yb_5Sb_3 to β-Yb_5Sb_3 transition from the Yb-Sb binary phase diagram. These observations with regards to the phase equilibria of Yb-Sb system were included in the present study's thermodynamic model. All crystallographic information of intermetallic phases in the current binary system are displayed in Table 1 and measured melting points and invariant reactions are collected in Table 2.

2.2 Thermochemical data

Sudavtsova et al. [28] conducted isoperibolic calorimetry studies in order to obtain the partial enthalpies of mixing in the liquid phase at different temperatures for both Yb and Sb, which are used in the current model. Pratt et al. [14] measured the enthalpy of formation of the YbSb compound to be -62±5 kJ/mol-atom using a direct-reaction calorimeter with certain modifications that were described in full detail in the report. This value was used in the thermodynamic modeling of Yb-Sb by Liu et al. [15] and resulted in the remaining compounds' enthalpies of formation to not be lower than ~65 kJ/mol-atom in the finalized assessment. Recently, Chong et al. [19] provided DFT-based predictions for 0 K and temperature dependent thermodynamic properties of the six intermetallic compounds in the Yb-Sb system. The results suggest that the formation enthalpies of the overall system should be more exothermic when compared to Pratt et al.'s measurement. Furthermore, it was discussed by Ferro et al. [29] that

multiple measurements of different rare-earth monoantimonides in Pratt et al.'s [14] report showed a large scatter when compared to other measurements in the literature and attributed it to the samples reacting with the tantalum cylinder used in the calorimeter. A comparison of DFT predictions provided by the Materials Project database alongside experimental work, including Pratt et al.'s measurements, is illustrated in Figure 1 (a) and (b). Figure 1 (a) shows enthalpy of formation measured by electromotive force (EMF) and calorimetry techniques between rare-earth (RE) mono-antimonides with the rocksalt structure alongside first-principles predictions from the Materials Project [30,31]. Figure 1 (b) displays enthalpy of formation DFT-based predictions and experimental measurements of a different rare-earth antimonide structure with RE_4Sb_3 (RE=rare earth) stoichiometry and $I\bar{4}3d$ spacegroup. The trends observed in both figures indicate an enthalpy of formation value that should be between -120 and -100 kJ/mol-atom rather than -60 kJ/mol-atom for the YbSb and Yb_4Sb_3 compounds. Furthermore, Figure 1 (a) also displays both the scatter in Pratt et al.'s measurements and its discrepancy with the measured enthalpies of formation of DySb and HoSb and the measurements that do agree with other experiments and therefore follow the -120 to -100 kJ/mol-atom trend proposed.

Although the trend in Figure 1 (a) suggested an enthalpy of formation in the range of -100 to -120 kJ/mol-atom for YbSb, the DFT predictions from Materials Project and Chong et al. [19,31] agreed with the measurement of -60 kJ/mol-atom from Pratt et al.[14]. This discrepancy motivated Chong et al.[19] to compare two different Yb pseudopotentials in order to observe their effect on the energetics of the binary system. Figure 2 presents the enthalpies of formation predicted by Chong et al. [19] of all six intermetallic phases predicted by DFT calculations using PBEsol as the functional with two different pseudopotentials which considered $5p^6 6d^2$ and $5p^6 6s^2 5d^1$ electrons as valence electrons, referred to in the study as Yb_2 and Yb_3, respectively. The results from the Yb_2 pseudopotential show a more negative enthalpy of

formation for most of the intermetallic compounds, which lied on their respective convex hull with exception of the orthorhombic Yb_5Sb_3 phase and the YbSb phase. However, the orthorhombic Yb_5Sb_3 phase should be above the convex hull since hexagonal Yb_5Sb_3 is more stable, as stated by Escamilla et al. [18]. The YbSb rocksalt structure; however is predicted to be 40 kJ/mol-atom above the convex hull and therefore suggests that the compound should not be present in the phase diagram, which does not agree with various experimental observations [1,13,25,32,33]. As discussed in other studies[25,34], the Yb in the YbSb compound adopts a trivalent state, which could explain the current discrepancy observed with the calculations with Yb_2. Figure 2 shows how the Yb_3 pseudopotential predicts the enthalpy of formation of the YbSb compound to be -100 kJ/mol-atom, which agrees more with the trend in (a) but not with (b) because it renders Yb_4Sb_3 above the convex hull, as well as $YbSb_2$, $Yb_{11}Sb_{10}$ and $Yb_{16}Sb_{11}$. A similar trend is observed when comparing the lattice parameters predicted by both pseudopotentials in Chong et al.'s [19] work. The lattice parameters of the YbSb compound predicted with the Yb_3 pseudopotential (6.03 Å) have a much better agreement with the experimental value (6.11 Å) than the prediction by the Yb_2 pseudopotential (6.38 Å), due to divalent nature of Yb [18,35]. However, the lattice parameter discrepancies between experiments and Yb_3 predictions of the other 5 intermetallic compounds have been calculated to be in the range of 2.8-11.4%. Based on these results and the suggestions in Chong et al.'s [19] study, the thermodynamic properties predicted with Yb_2 pseudopotential will be used to model the Gibbs energy functions of Yb_5Sb_3, $Yb_{16}Sb_{11}$, $Yb_{11}Sb_{10}$ and $YbSb_2$.

Chong et al.'s [19] work could not provide reliable thermodynamic properties of the ordered FCC YbSb structure since the phonon supercell approach would predict extensive imaginary modes, suggesting instability. The improved lattice parameter agreement of the YbSb compound predicted with the Yb_3

pseudopotential suggests that it could be the key to approach this issue. Therefore, it is hypothesized in this work that Yb_3 pseudopotential can be used to predict temperature dependent thermodynamic properties of the YbSb rocksalt structure with no formation of imaginary modes. The resulting predictions will be used to parameterize the temperature dependent Gibbs energy function of the compound and ultimately include it in the current database.

3 Methodologies

3.1 First-principles calculations

DFT-based first-principles calculations were carried out to predict 0K formation energies and temperature dependent thermodynamic properties of the Yb-Sb compounds, using the Vienna ab initio simulation package (VASP)[36] with GGA and PBEsol. Core electrons were treated with the projector augmented wave method (PAW) [37]. The Methfessel-Paxton method with a smearing width of 0.1 was employed to smear the electronic states for structural relaxations. The plane-wave cutoff energy was set as 450 eV for crystal relaxation and 520 eV for 0 K static energy calculation. Around 2800 *k*-points per reciprocal atom [38,39] was used. The total energy calculations were conducted with the tetrahedron method and Blöchl corrections [40]. The pseudopotential chosen for Sb followed the recommendation from VASP.5.2. The Yb_3 pseudopotential with $5p^6 6s^2 5d^1$ valence electrons is utilized for final calculations, meaning that one of the $4f^{14}$ electrons is delocalized into the 5d shell as proposed by Svane et al. [34].

Based on the quasiharmonic approach, the Helmholtz energy of a stoichiometric phase can be represented as function of temperature (T) and volume (V), composing of three energetic contributions

$$\boldsymbol{F(V,T) = E_0(V) + F_{Vib}(V,T) + F_{ele}(V,T)} \quad \text{Eq. 1}$$

where E_0(V) represents the 0 K static ground state energy, $F_{vib}(V,T)$ the vibrational energy of the lattice ions, and $F_{ele}(V,T)$ the energy due to thermally excited electrons [41]. The Helmholtz energy can be converted into the Gibbs energy through the addition of a term PV (P is the pressure) which is a negligible amount at ambient condition.

The $E_0(V)$ contributions for the compound and all end-members are determined through the 4 parameter Birch-Murnaghan (BM4) fitting shown below [23]

$$\boldsymbol{E_0(V) = a + bV^{-\frac{2}{3}} + cV^{-\frac{4}{3}} + dV^{-2}} \quad \text{Eq. 2}$$

where a, b, c, and d are fitting parameters. The BM4 fitting used data from 6 different volumes. The vibrational energy contribution of the lattice can be calculated through the quasiharmonic phonon calculations based on the supercell method [23] as,

$$\boldsymbol{F_{Vib}(V,T) = K_bT \int_0^\infty \ln\left[2sinh\frac{\hbar\omega}{2K_bT}\right] g(\omega,V) d\omega} \quad \text{Eq. 3}$$

where g(ω,V)[41] is the phonon density of states as a function of volume (V) and frequency (ω) [41]. The software phonopy [42] was used to obtain the temperature dependent properties.

3.2 Thermodynamic modeling

The Gibbs energy functions of pure Yb and Sb were obtained from the Scientific Group Thermodata Europe (SGTE) database [43]. The $YbSb_2$, YbSb, $Yb_{11}Sb_{10}$, Yb_4Sb_3, $Yb_{16}Sb_{11}$ and Yb_5Sb_3 phases were

modeled as stoichiometric compounds. The liquid phase was modeled with the associate model to describe strong short-range interactions that are believed to exist due to the high congruent melting point of the Yb_4Sb_3 compound as generally performed in the literature [44,45] and supported by the recent ab initio molecular dynamic simulations for the Ba-Bi system.[46]

The Gibbs energy of the $YbSb_2$, YbSb, $Yb_{11}Sb_{10}$, Yb_4Sb_3, $Yb_{16}Sb_{11}$ and Yb_5Sb_3 above room temperature are described using the SGTE model as follows

$$\boldsymbol{G^{Yb_x Sb_y} - H^{SER} = a + bT + cT\,ln\,T + dT^2 + eT^{-1} + fT^3} \qquad \text{Eq. 4}$$

where *a*, *b*, *c*, *d*, *e* and *f* are the model parameters[47] evaluated from the temperature dependent Gibbs energy predicted by the quasiharmonic approximation from Chong et al., [19] and H^{SER} refers to the enthalpies of face centered cubic (fcc) Yb and rhombohedral-Sb at 298.15K and 1 bar.

The large difference in melting point between Yb_4Sb_3 and its constituents indicate a strong interaction between Yb and Sb in the liquid phase. The associate chosen for this system is Yb_4Sb_3, in accordance with the composition of the highest melting compound and the compound melting congruently, which is a reasonable assumption to make based on these facts [48]. The Gibbs energy function of the liquid phase is expressed as

$$\boldsymbol{G_m^{Liq}(T, y_i) = \sum_{i=1}^{3} y_i G_i^L + RT \sum_{i=1}^{3} y_i ln y_i + \sum_{i=1}^{2} \sum_{j>i}^{3} y_i y_j \sum_{v=0}^{n} L_{i,j}^{v,L} (y_i - y_j)^v} \qquad \text{Eq. 5}$$

where R, T and y_i are the gas constant, temperature and the mole fraction of specie *i* in the liquid phase respectively. The i and j represent the 3 species Sb, Yb, and Yb_4Sb_3 of the binary system in the alphabetic order. In the ${}^0G_i^L$ parameter represents the Gibbs energy of pure Sb, Yb and the Yb_4Sb_3 specie in the liquid phase. The interaction parameter, $\boldsymbol{L_{i,j}^{v,L}}$, is of the form as follows

$$^{v}\boldsymbol{L}_{\boldsymbol{i,j}}^{\boldsymbol{Liq}} = {}^{\boldsymbol{v,Liq}}\boldsymbol{A} + {}^{\boldsymbol{v,Liq}}\boldsymbol{BT} \qquad \text{Eq. 6}$$

where $^{v}L_{i,j}^{Liq}$ is the vth interaction parameter between species i and j, and the model parameters $^{v,Liq}A$ and $^{v,Liq}B$ are evaluated based on the experimental thermochemical and phase equilibria data related to the liquid state. The Gibbs energy function of the Yb_4Sb_3 specie is described as

$$\boldsymbol{G}_{\boldsymbol{Yb_4Sb_3}}^{\boldsymbol{Liq}}(\boldsymbol{T}) = \frac{\boldsymbol{4}}{\boldsymbol{7}}\boldsymbol{G}_{\boldsymbol{Yb}}^{\boldsymbol{L}} + \frac{\boldsymbol{3}}{\boldsymbol{7}}\boldsymbol{G}_{\boldsymbol{Sb}}^{\boldsymbol{L}} + \boldsymbol{A} + \boldsymbol{BT} + \boldsymbol{CTlnT} \qquad \text{Eq. 7}$$

where A, B and C are modeled to experimental and thermochemical experiments available in the literature. The first-principles data and experimental data are combined for parameter evaluation by calling the PARROT module in the Thermo-Calc software.[49]

4 Results and discussion

4.1 DFT-based first-principles calculations

Figure 2 has strong implications about the valence state of Yb as its compositions change throughout this binary system. Figure 2 suggests that the divalent structures in the system are $Yb_{11}Sb_{10}$, Yb_4 Sb_3, $Yb_{16}Sb_{11}$, Yb_5Sb_3, $YbSb_2$ since these structures lie on the convex hull and have good lattice parameter agreement [19] with experiments when the Yb_2 pseudopotential is applied in the DFT calculations. These claims can be further supported by Bodnar et al.[35] that the valence state of Yb in the $Yb_{11}Sb_{10}$, Yb_5Sb_3 and $YbSb_2$ structure is +2 due to the magnetic susceptibility of the structure through the Faraday technique. This measurement can be further supported by the fact that the $Yb_{11}Sb_{10}$ and Yb_5Sb_3 can be found in other alkaline rare-earth (Sr,Ba) pnictide (Sb,Bi,As) systems where the alkaline rare-earth metals tend to be divalent. By this logic, it is reasonable to assume that Yb is divalent in the $Yb_{16}Sb_{11}$ structure since it is found in the aforementioned systems as well. Bodnar et al. [35] also measured that the Yb_4Sb_3 compound contained both +2 and +3 Yb atoms, which is further supported by Suga et al.'s

[50] study, which determined that average valence of Yb to be ~+2.3 through X-ray photoemission spectroscopy. This could imply that formation of the structure could be more exothermic if the Yb pseudopotential could handle these multi-valent cases. These experimental observations agree with the aforementioned computational observations in Chong et al.'s [19] work and illustrate the need for a pseudopotential that can handle such multivalence phenomena in order to more correctly model the stability of systems that show this electronic behavior.

Figure 3 and Figure S 1 in the supplementary information present the electronic density of states and electronic band dispersion plot of the YbSb compound, respectively. These figures show that some of the states were partially filled with respect to the Fermi level at 0 K, which suggest that the compound should in fact be a conductor. Even though Abdusalyamova et al. [51] suggested that YbSb had a bandgap of 0.8 eV, a more recent experimental study conducted by Kawamura et al. [32] indicated that YbSb was metallic in nature, which agrees with the DFT-based prediction.

The dielectric tensor and Born effective charges of the YbSb compound were computed in the present work and presented in Table S 2 and Table S 3 of the supplementary information, respectively. The values suggest that the structure has dipole-dipole interactions. Figure 4 (a) and (b) show the phonon dispersions and the phonon density of states of the YbSb compound predicted using the Yb_3 pseudopotential with a 64 atom supercell. The phonon dispersions have 6 phonon bands based on the 2-atom YbSb primitive cell without imaginary modes, demonstrating the importance of treating one of the $4f^{14}$ electrons as delocalized by using the Yb_3 pseudopotential. The removal of imaginary modes suggests that Yb indeed has a valency of +3 in the YbSb compound. The valency of the structure

comparing Yb_3 and Yb_2 pseudopotentials was further studied through Bader charge analysis as well as Born effective charges, which are presented in the supplementary material.

The temperature dependent heat capacity of YbSb predicted by the quasiharmonic approximation with the Yb_3 pseudopotential is compared with the Neumann-Kopp prediction in Figure 5, alongside the heat capacities of its elemental constituents (Yb and Sb) provided by SGTE. The kink at 553 K is present in both the Neumann-Kopp prediction and the heat capacity of Yb. The temperature at which this occurs is well below the fcc-bcc transformation (1038 K) and the melting point of Yb (1097 K). The possibility of a magnetic transition was also implausible based on the study of Lock et al. [52], who deemed the majority of atoms to have zero magnetic moment. The study conducted by Berg et al. [53], of which the SGTE model is based on, proposed that the kink could be related to the excitation of electrons in the 14*f* shell into the conduction band. This hypothesis; however, is yet to be tested and published in the literature.

4.2 Thermodynamic modeling

The temperature dependent thermodynamic properties of the YbSb phase, predicted by the Yb_3 pseudopotential, were used to model its Gibbs energy function. The Gibbs energy models of other intermetallic compounds are based on the thermodynamic properties predicted by Chong et al. [19] using the Yb_2 pseudopotential. Figure 6 compares the enthalpy of formation data in the system at 298.15 K between the model by Liu et al. [15] and the current work. As it can be see, this study's convex hull is lower in energy and is based on more data points rather than just Pratt et al.'s[14] work. As mentioned earlier in the manuscript, the enthalpy of formation of YbSb calculated with the Yb_3 pseudopotential

will not be considered in the current modeling work, hence, was not plotted in Figure 6. The thermodynamic model shows good agreement with the DFT predictions, with the largest discrepancy being a 3.6kJ (4.2%) difference between the model and the DFT prediction for $Yb_{11}Sb_{10}$. Model parameters of all phases are collected in Table 2. The comparison of the thermodynamic properties between CALPHAD database and the predicted DFT calculations can be found in the supplementary information.

The Yb_4Sb_3 associate is considered for the liquid phase in the present study to describe the short-range ordering. Figure 7 shows the fractions of species in liquid at 1973 K, above the congruent melting point of Yb_4Sb_3. As it can be observed, the closer the composition is to the molar fraction of 0.6, the greater the amount of the Yb_4Sb_4 associate, indicating the strong interactions between the Yb and Sb to form the associate. Figure 8 (a) and (b) presents the partial enthalpy of mixing energies of Yb and Sb in the liquid state measured by Sudavtsova et al. [28] and from the CALPHAD modeling by Liu et al. [15] in comparison with the present work. As it can be seen in Figure 8 (a), the experimental partial enthalpy of mixing differs between 50-80kJ/mol from Liu's model and 5-20kJ/mol from the present work. Though the difference between Sudavtsova et al.'s [28] experiments and the current model's calculations are still relatively high , it is believed that the discrepancies are acceptable due to the scatter of datapoints and lack of error bars in the data. Figure 8 (b) presents a similar result except there is a much larger scatter in the measurements by Sudavtsova et al.[28] (1-80 kJ/mol). Nevertheless, the present model has better agreement with the experiments than Liu's model.

Figure 9 (a) shows the phase diagram calculated from the present thermodynamic model. As it can be seen the invariant reactions observed by Abulkhaev et al. [13] were reproduced within the proposed error

range. The invariant reaction between the high temperature and low temperature of Yb_5Sb_3 at 1405°C is not considered in the present work as discussed above. The melting point of $Yb_{16}Sb_{11}$ was chosen to be an average of the melting points of Yb_5Sb_3 and Yb_4Sb_3 at 1627°C. The invariant reactions and melting points calculated from the present model can be found in Table 2. Figure 9 (b) shows the Yb-Sb phase diagram calculated with Liu et al.'s database superimposed on this current work's model. As it can be seen there is good agreement of the liquidus lines and the invariant reactions between both models. The largest discrepancy can be observed on the Sb rich side between x(Sb) of 0.7 and 0.9, where Liu et al.'s phase diagram has liquids that is lower in temperature by ~50 K, which has minimal impact on the agreement with the experimental data as shown in Figure 9 (a).

Figure 10 (a) presents the proposed phase diagram by Bodnar et al. [25], in which it was observed that Yb_5Sb_3 was in equilibrium with the gas phase and not the liquid, in contrast to the observations by Abulkhaev's work [13]. With the Gibbs energy of the gas phase from the SGTE SSUB5 thermodynamic database [43], Figure 10 (b) shows that on the Yb rich side there is a temperature range between 1200-1450°C where the gas phase is in equilibrium with Yb_5Sb_3, in agreement with the observations by Bodnar et al.[25] Furthermore, it predicts that $Yb_{16}Sb_{11}$ is also in equilibrium with the gas phase, and Yb_4Sb_3 melts congruently as also observed by Bodnar et al.[25]. This is an important finding, since it is known that the vapor pressure of Yb is quite high [21] and its vaporization temperature is 1196°C and yet it is not discussed in Abulkhaev's study [13]. Figure 10 (c) presents the vapor pressure of Yb and Sb at 1400°C as a function of composition of Sb. The Sb vapor pressure plotted, represented by the solid black line, is the summation of all 4 of the vapor pressures of the individual Sb gas species present in the database. The red dashed line represents the vapor pressure of Yb at x_{Sb}=~0.6, the vapor pressure of ~30 Pa, indicating substantial sublimation and the need to verify the compositions after the DTA experiment,

which were not carried out in either work [13,25]. More experimental work on the equilibria data in the Yb-Sb system is desirable.

5 Conclusions

The Yb-Sb binary system has been remodeled using the CALPHAD approach based on available experimental data in the literature and first-principles calculations in the present work. Based on experimental and computational evidence, the $Yb_{16}Sb_{11}$ compound is included and the high temperature transformation of Yb_5Sb_3 is removed. Finite temperature predictions the phonon method of the YbSb compound with two different Yb pseudopotentials are compared. The liquid short-range order in the system is described through the associate model. The resulting thermodynamic model is compared with the thermochemical and phase equilibria data found in the literature with satisfactory agreement. This model will be used to develop the thermodynamic model of Mn-Sb-Yb ternary system with the $Yb_{14}MnSb_{11}$ Zintl phase.

6 References

[1] A. Yamamoto, J. Takeda, T. Koyama, T. Mito, S. Wada, I. Shirotani, C. Sekine, Evidence for an antiferroquadrupolar ordering in YbSb probed by ^{121}Sb and ^{123}Sb nuclear magnetic resonances, Phys. Rev. B. 70 (2004) 220402. doi:10.1103/PhysRevB.70.220402.

[2] L.L. Zhao, S. Lausberg, H. Kim, M.A. Tanatar, M. Brando, R. Prozorov, E. Morosan, Type-I superconductivity in YbSb 2 single crystals, Phys. Rev. B - Condens. Matter Mater. Phys. 85 (2012) 1–6. doi:10.1103/PhysRevB.85.214526.

[3] Y. Lu, J. Wang, J. Li, J. Wu, S. Kanno, T. Tada, H. Hosono, Realization of Mott-insulating electrides in dimorphic Yb_5Sb_3, Phys. Rev. B. 98 (2018) 1–12. doi:10.1103/PhysRevB.98.125128.

[4] I.G. Vasilyeva, R.E. Nikolaev, M.N. Abdusaljamova, S.M. Kauzlarich, Thermochemistry study and improved thermal stability of $Yb_{14}MnSb_{11}$ alloyed by Ln3+ (La-Lu), J. Mater. Chem. C. 4 (2016) 3342–3348. doi:10.1039/c6tc00178e.

[5] S. Ohno, A. Zevalkink, Y. Takagiwa, S.K. Bux, G.J. Snyder, Thermoelectric properties of the $Yb_9Mn_{4.2-xZn_x}Sb_9$ solid solutions, J. Mater. Chem. A. 2 (2014) 7478–7483. doi:10.1039/c4ta00539b.

[6] A. He, S.K. Bux, Y. Hu, D. Uhl, L. Li, D. Donadio, S.M. Kauzlarich, Structural Complexity and High Thermoelectric Performance of the Zintl Phase: $Yb_{21}Mn_4Sb_{18}$, Chem. Mater. (2019). doi:10.1021/acs.chemmater.9b02671.

[7] S.R. Brown, S.M. Kauzlarich, F. Gascoin, G. Jeffrey Snyder, $Yb_{14}MnSb_{11}$: New high efficiency thermoelectric material for power generation, Chem. Mater. 18 (2006) 1873–1877. doi:10.1021/cm060261t.

[8] A. Möchel, I. Sergueev, H.C. Wille, F. Juranyi, H. Schober, W. Schweika, S.R. Brown, S.M.

Kauzlarich, R.P. Hermann, Lattice dynamics in the thermoelectric Zintl compound $Yb_{14}MnSb_{11}$, Phys. Rev. B - Condens. Matter Mater. Phys. 84 (2011) 1–10. doi:10.1103/PhysRevB.84.184303.

[9] A.S. Guloy, F. Gascoin, A. Chamoire, J.C. Tedenac, G.J. Snyder, Synthesis and thermoelectric properties of $YbSb_2Te_4$, Phys. Status Solidi - Rapid Res. Lett. 1 (2007) 265–267. doi:10.1002/pssr.200701228.

[10] I. Mili, H. Latelli, T. Ghellab, Z. Charifi, H. Baaziz, F. Soyalp, The study of structural, electronic and thermoelectric properties of $Ca_{1-x}Yb_xZn_2Sb_2$ (x = 0, 0.25, 0.5, 0.75, 1) Zintl compounds, Int. J. Mod. Phys. B. 35 (2021) 1–18. doi:10.1142/S0217979221501009.

[11] S.-W. Chen, J.-W. Chen, P.-H. Lin, Liquidus projection of Co-Sb-Yb ternary system, Mater. Lett. 182 (2016) 36–38. doi:10.1016/j.matlet.2016.06.068.

[12] S.K. Bux, J.-P. Fleurial, T. Caillat, B. Chun, Y. Li, K. Star, S. Firdosy, V. Ravi, C.-K. Huang, B. Cheng, P. Gogna, J. Ma, P. Von Allmen, T. Vo, Engineering of Novel Thermoelectric Materials and Devices for Next Generation, Long Life, 20% Efficient Space Power Systems, (n.d.). doi:10.2514/6.2013-3927.

[13] V.D. Abulkhaev, Phase relations and properties of alloys in the Yb-Sb system, Inorg. Mater. 39 (1997) 47–49. doi:10.1023/A:1021887102509.

[14] J.N. Pratt, C. K.S., Thermodynamic studies of some rare-earth alloys, 1970.

[15] X.J. Liu, S.X. Gan, Z.S. Li, C.P. Wang, A.T. Tang, F.S. Pan, Thermodynamic assessment of the Ho-Sb and Sb-Yb systems, Calphad Comput. Coupling Phase Diagrams Thermochem. 37 (2012) 132–136. doi:10.1016/j.calphad.2012.02.004.

[16] E.A. Leon-Escamilla, W.-M. Hurng, E.S. Peterson, J.D. Corbett, Synthesis, Structure, and Properties of $Ca_{16}Sb_{11}$, a Complex Zintl Phase. Twelve Other Isotypic Compounds Formed by

Divalent Metals and Pnictogens, Inorg. Chem. 36 (1997) 703–710. doi:10.1021/ic961035w.

[17] V. Ponnambalam, X. Gao, S. Lindsey, P. Alboni, Z. Su, B. Zhang, F. Drymiotis, M.S. Daw, T.M. Tritt, Thermoelectric properties and electronic structure calculations of low thermal conductivity Zintl phase series $M_{16}X_{11}$ (M=Ca and Yb; X=Sb and Bi), J. Alloys Compd. 484 (2009) 80–85. doi:10.1016/j.jallcom.2009.04.131.

[18] Leon-Escamilla E. Alejandro, Corbett John D., Hydrogen stabilization. Nine isotypic orthorhombic A_5Pn_3H phases (among A=Ca, Sr, Ba, Sm, Eu, Yb; Pn=Sb, Bi) formerly described as binary β Yb_5Sb_3 type compounds, J. Alloys Compd. 265 (1998) 104–114.

[19] X. Chong, J. Paz Soldan Palma, Y. Wang, F. Drymiotis, K.E. Star, J.-P. Fleurial, V.A. Ravi, Z.-K. Liu, Ab initio thermodynamics of the Yb-Sb system: applied to predict stability of high temperature thermoelectric Zintl phase, ACta Ma. (2021).

[20] J. Paik, E. Brandon, T. Caillat, R. Ewell, J.-P. Fleurial, Life Testing of $Yb_{14}MnSb_{11}$ for High Performance Thermoelectric Couples, Proc. Nucl. Emerg. Technol. Sp. (2011).

[21] J.A. Nesbitt, Rate of Sublimation of $Yb_{14}MnSb_{11}$, a Thermoelectric Material for Space Power Applications, J. Electron. Mater. 43 (2014). doi:10.1007/s11664-014-3261-8.

[22] Z.K. Liu, First-Principles calculations and CALPHAD modeling of thermodynamics, J. Phase Equilibria Diffus. 30 (2009) 517–534.

[23] S.-L. Shang, Y. Wang, D. Kim, Z.-K. Liu, First-principles thermodynamics from phonon and Debye model: Application to Ni and Ni_3Al, Comput. Mater. Sci. 47 (2010) 1040–1048. doi:10.1016/j.commatsci.2009.12.006.

[24] H. Xia, F. Drymiotis, C.-L. Chen, A. Wu, G.J. Snyder, Bonding and interfacial reaction between Ni foil and n-type PbTe thermoelectric materials for thermoelectric module applications, J. Mater. Sci. 49 (2014) 1716–1723. doi:10.1007/s10853-013-7857-9.

[25] R.E. Bodnar, H. Steinfink, The Phase Equilibriums and Crystal Chemistry of the Intermediate Phases in the Ytterbium-Antimony System, Inorg. Chem. 6 (1967) 327–330. doi:10.1021/ic50048a030.

[26] H.L. Clark, H.D. Simpson, H. Steinfink, The Crystal Structure of $Yb_{11}Sb_{10}$, Inorg. Chem. 9 (1970) 1962–1964. doi:10.1021/ic50090a049.

[27] E. Alejandro Leon-Escamilla, J.D. Corbett, Hydrogen in polar intermetallics. Binary pnictides of divalent metals with Mn_5Si_3-type structures and their isotypic ternary hydride solutions, Chem. Mater. 18 (2006) 4782–4792. doi:10.1021/cm0612191.

[28] S. Sudavtsova, M. Shevchenko, M. Ivanov, V. Berezutskii, V. Kudin, Ky. Pastushenko, K. Yu Pastushenko, Thermodynamic Properties of Alloys of the Binary Sb–Yb System, Russ. J. Phys. Chem. A. 91 (2017) 1174–1182. doi:10.1134/S0036024417070287.

[29] R. Ferro, G. Borzone, G. Cacciamani, N. Parodi, Thermodynamics of rare earth alloys: Systematics and experimental, Thermochim. Acta. 314 (1998) 183–204. doi:10.1016/s0040-6031(98)00266-4.

[30] M.E. Schlesinger, Thermodynamic properties of solid binary antimonides, Chem. Rev. 113 (2013) 8066–8092. doi:10.1021/cr400050e.

[31] A. Jain, S.P. Ong, G. Hautier, W. Chen, W.D. Richards, S. Dacek, S. Cholia, D. Gunter, D. Skinner, G. Ceder, K.A. Persson, Commentary: The materials project: A materials genome approach to accelerating materials innovation, APL Mater. 1 (2013). doi:10.1063/1.4812323.

[32] A. Kawamura, Y. Hu, S.M. Kauzlarich, Synthesis and Thermoelectric Properties of the YbTe-YbSb System, 45 (n.d.). doi:10.1007/s11664-015-4202-x.

[33] R. Mishra, R. Pöttgen, R.-D. Hoffmann, T. Fickenscher, M. Eschen, H. Trill, B.D. Mosel, Ternary Antimonides YbTSb (T = Ni, Pd, Pt, Cu, Ag, Au) – Synthesis, Structure, Homogeneity

Ranges, and 121 Sb Mössbauer Spectroscopy, Zeitschrift Für Naturforsch. B. 57 (2002) 1215–1223.

[34] A. Svane, W.M. Temmerman, Z. Szotek, L. Petit, P. Strange, H. Winter, Ab initio theory of valency in ytterbium compounds, Phys. Rev. B - Condens. Matter Mater. Phys. 62 (2000) 13394–13399. doi:10.1103/PhysRevB.62.13394.

[35] R.E. Bodnar, H. Steinfink, K.S.V.L. Narasimhan, Magnetic and Electrical Properties of Some Yb-Sb Phases, J. Appl. Phys. 39 (1968) 1485–1489.

[36] G. Kresse, J. Furthmüller, Efficiency of ab-initio total energy calculations for metals and semiconductors using a plane-wave basis set, Comput. Mater. Sci. (1996).

[37] P.E. Blöchl, Projector augmented-wave method, Phys. Rev. B. 50 (1994) 17953–17979. doi:10.1103/PhysRevB.50.17953.

[38] G. Kresse, J. Furthmüller, Efficient iterative schemes for ab initio total-energy calculations using a plane-wave basis set, Phys. Rev. B. 54 (1996). https://journals.aps.org/prb/pdf/10.1103/PhysRevB.54.11169 (accessed November 6, 2017).

[39] M. Methfessel, A.T. Paxton, High-precision sampling for Brillouin-zone integration in metals, Phys. Rev. B. 40 (1989).

[40] P.E. Blöchl, O. Jepsen, O.K. Andersen, Improved tetrahedron method for Brillouin-zone integrations, Phys. Rev. B. 49 (1994) 16223–16233. https://journals.aps.org/prb/pdf/10.1103/PhysRevB.49.16223 (accessed June 24, 2019).

[41] Y. Wang, Z.-K. Liu, L.-Q. Chen, Thermodynamic properties of Al, Ni, NiAl, and Ni_3Al from first-principles calculations, Acta Mater. 52 (2004) 2665–2671.

[42] T. Atsushi, I. Tanaka, First principles phonon calculations in materials science, Scr. Mater. 108 (2015) 1–5. doi:10.1016/j.scriptamat.2015.07.021.

[43] A.T. Dinsdale, SGTE Data for Pure Elements, CALPHAD. 15 (1991) 317–425.

[44] F. Sommer, Association Model for the Description of Thermodynamic Functions of Liquid Alloys. II.--Numerical Treatment and Results, Z. Met. 73 (1982) 77–86.

[45] J. Liu, P.W. Guan, C.N. Marker, N.D. Smith, N. Orabona, S.L. Shang, H. Kim, Z.K. Liu, Thermodynamic properties and phase stability of the Ba-Bi system: A combined computational and experimental study, J. Alloys Compd. 771 (2019) 281–289. doi:10.1016/j.jallcom.2018.08.324.

[46] J. Ma, S.-L. Shang, H. Kim, Z.-K. Liu, An ab initio molecular dynamics exploration of associates in Ba-Bi liquid with strong ordering trends, Acta Mater. 190 (2020) 81–92. doi:10.1016/j.actamat.2020.03.024.

[47] B.-C. Zhou, S.-L. Shang, Z.-K. Liu, First-principles calculations and thermodynamic modeling of the Sn-Sr and Mg-Sn-Sr systems, Calphad. 46 (2014) 237–248. doi:10.1016/j.calphad.2014.04.003.

[48] R. Arroyave, Z.K. Liu, Thermodynamic modelling of the Zn-Zr system, Calphad Comput. Coupling Phase Diagrams Thermochem. 30 (2006) 1–13. doi:10.1016/j.calphad.2005.12.006.

[49] J.-O. Andersson, T. Helander, L. Höglund, P. Shi, B. Sundman, THERMO-CALC & DICTRA, Computational Tools For Materials Science, Calphad. 26 (2002) 273–312. http://www.thermocalc.se/ (accessed July 12, 2018).

[50] S. Suga, S. Ogawa, H. Namatame, M. Taniguchi, A. Kazizaki, T. Ishii, A. Fujimori, S.-J. Oh, H. Kato, T. Miyahara, A. Ochiai, T. Suzuki, T. Kasuyam, XPS and UPS Studies of Valence Fluctuation and Surface States of Yb4As3, Yb4Sb3 and Yb4Bi3, J. Phys. Soc. Japan. 58 (1989) 4534–4543.

[51] M.N. Abdusalyamova, H.S. Shokirov, O.I. Rakhmatov, Investigation of the rare earth

monoantimonides, J. Less-Common Met. 166 (1990) 221–227. doi:10.1016/0022-5088(90)90003-3.

[52] J.M. Lock, The Magnetic Susceptibility of Ytterbium from 1.3°K to 300°K, Proc. Phys. Soc. Sect. B. 70 (1957).

[53] J.R. Berg, A.H. Daane, The high temperature heat contents and related thermodynamic properties of lanthanum, praseodymium, europium, ytterbium and yttrium, Iowa State University of Science and Technology, 1961.

[54] G. Rossi, A. Barski, Electron-emission processes following 5p photoexcitation in fcc Yb, Phys. Rev. B. 32 (1985).

Acknowledgments

This research was carried out at the Jet Propulsion Laboratory, California Institute of Technology, and The Pennsylvania State University, under a contract with the National Aeronautics and Space Administration. This research received funding from the Pennsylvania State University's Institute for CyberScience through the ICS Seed Grant Program (Paz Soldan Palma, Chong, Wang, and Liu) as well as finical support from the U. S. National Science Foundation (NSF) with Grant No. CMMI-2226976 (Shang and Liu). Jorge Paz Soldan Palma would like to thank Dr. Austin Ross and Mr. Brandon Bocklund for all their helpful advice and discussions. First-principles calculations were performed partially on the Roar supercomputer at the Pennsylvania State University's Institute for Computational and Data Sciences (ICDS), partially on the resources of the National Energy Research Scientific Computing Center (NERSC) supported by the U.S. Department of Energy Office of Science User Facility operated under Contract No. DE-AC02-05CH11231, and partially on the resources of the Extreme Science and Engineering Discovery Environment (XSEDE) supported by NSF with Grant No. ACI-1548562.

Table 1 Crystallographic data of the intermetallic phases in the Yb-Sb binary system. The table presents the enthalpy of formation values predicted by DFT with the PBEsol functional alongside Yb_2 pseudopotential from Chong et al.'s work [19] as well as the calorimetric measurement of YbSb by Pratt et al. [14]. The table presents the charge of Yb measured and predicted in different structures.

Phases	**Pearson Symbol**	**Space Group**	**Mehod**	**ΔH (kJ/mol-atom)**	**Ref**	**Yb charge**	**Ref**
Yb	cF8	$Fm\bar{3}m$				2	[54]
Yb_5Sb_3	hP16	$p6_3/mcm$	DFT	-98.48	[19]	2	[35]
$Yb_{16}Sb_{11}$	tP56	$P\bar{4}21m$	DFT	-101.94	[19]	-	
Yb_4Sb_3	cl28	$I\bar{4}3d$	DFT	-100.24	[19]	2.34	[35,50]
$Yb_{11}Sb_{10}$	tl84	$I4/mmm$	DFT	-96.70	[19]	2	[35]
YbSb	cF8	$Fm\bar{3}m$	Experiment	-62	[14]	3	[34,35]
			DFT	-64.03	[19]		
$YbSb_2$	oS12	$Cmcm$	DFT	-68.29	[19]	2	[35]
Sb	hR6	$R\bar{3}m$				N/A	

Table 2 Invariant reactions in the Yb-Sb system

Reaction type	Reaction	T/K	Method	Reference
Eutectic	Liquid ↔ Rhombohedral+$YbSb_2$	893±10	Experimental	[13]
		880	Calculated	This work
Peritectic	Liquid+YbSb ↔ $YbSb_2$	1118±15	Experimental	[25]
		1078±5	Experimental	[13]
		1080	Calculated	This work
Peritectic	Liquid+$Yb_{11}Sb_{10}$ ↔ YbSb	1348±10	Experimental	[25]
		1340	Calculated	This work
Peritectic	Liquid+ Yb_4Sb_3↔ $Yb_{11}Sb_{10}$	1678±10	Experimental	[13]
		1684	Calculated	This work
Congruent	Liquid ↔ Yb_4Sb_3	1813±10	Experimental	[25]
		1953±15	Experimental	[13]
		1963	Calculated	This work
Peritectic	Liquid+ Yb_4Sb_3 ↔ $Yb_{16}Sb_{11}$	1900	Calculated	This work
Peritectic	Liquid+ $Yb_{16}Sb_{11}$ ↔ Yb_5Sb_3	1813±15	Experimental	[13]
		1823	Calculated	This work

Eutectic	Liquid ↔ Yb_5Sb_3+ BCC_A2	1083±5	Experimental	[13]
		1063	Calculated	This work
Peritectic	BCC_A2↔FCC_A1+Yb_5Sb_3	1038±5	Experimental	[13]
		1033	Calculated	This work

Table 3 The parameters of the present thermodynamic modeling of Yb-Sb system

Phase and model	Model parameters
Liquid, (Sb,Yb_4Sb_3, Yb)	$G^{Yb_4Sb_3} - 74000 + 0.2T + 0.571428G_{Yb}^{Liq} + 0.428571G_{Sb}^{Liq}$ ${}^0L_{Sb,Y_4Sb_3}^{Liq} = -55000 + 14T$ ${}^1L_{Sb,Y_4Sb_3}^{Liq} = 24000$ ${}^0L_{Yb,Yb_4Sb_3}^{Liq} = -41500 + 25T$ ${}^1L_{Yb,Y_4Sb_3}^{Liq} = 20500 - 4T$
BCC (Sb,Yb)	${}^0L_{Sb,Yb}^{BCC} = -209850$
FCC (Sb,Yb)	${}^0L_{Sb,Yb}^{FCC} = -210825$
$YbSb_2$	$G^{YbSb_2} - H^{SER} = -230740 + 409.9T - 81.98T\ ln(T) - 0.00395T^2 + 207313T^{-1} - 2.17 \times 10^{-6}T^3$ (J/mol-formula)
YbSb	$G^{YbSb} - H^{SER} = -214850 + 247.92T - 50.68T\ ln(T) - 0.000482T^2 + 79696T^{-1} - 3.23 \times 10^{-7}T^3$ (J/mol-formula)
$Yb_{11}Sb_{10}$	$G^{Yb_{11}Sb_{10}} - H^{SER} = -2282010 + 2736.8T - 556T\ ln(T) + 0.00432T^2 + 1040607T^{-1} - 9.18 \times 10^{-6}T^3$ (J/mol-formula)
Yb_4Sb_3	$G^{Yb_4Sb_3} - H^{SER} = -766156 + 891.8T - 184T\ ln(T) + 0.00162T^2 + 236985T^{-1} - 3.46 \times 10^{-6}T^3$ (J/mol-formula)
$Yb_{16}Sb_{11}$	$G^{Yb_{16}Sb_{11}} - H^{SER} =$ -2960444 $+ 3332T - 696T\ ln(T) + 0.00408T^2 + 957485T^{-1} - 7.77 \times 10^{-6}T^3$ (J/mol-formula)
Yb_5Sb_3	$G^{Yb_5Sb_3} - H^{SER} = -851897 + 989.6T - 205T\ ln(T) - 0.00312T^2 + 218237T^{-1} - 2.04 \times 10^{-6}T^3$ (J/mol-formula)

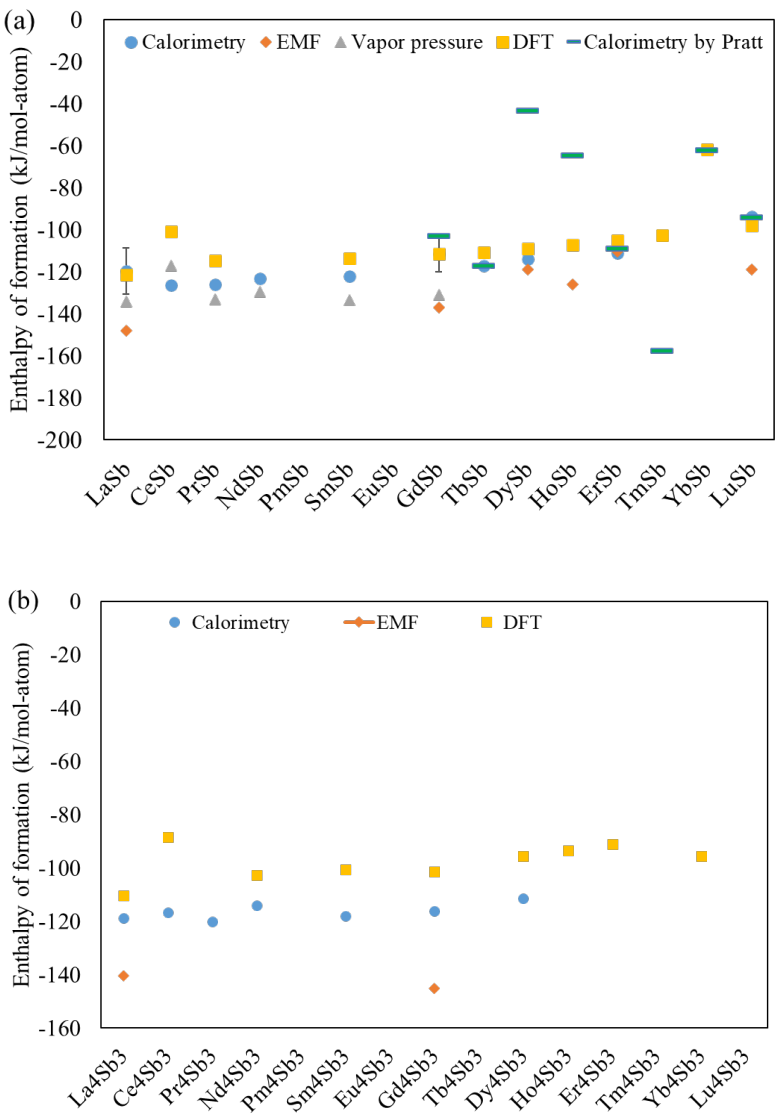

Figure 1 (a) Measured [14,30] and DFT predicted [31] enthalpies of formation of compounds with the rocksalt rare-earth-pnictide ReSb structure (b) and the Re_4Sb_3 $I\bar{4}3d$ structure (Re=Rare-earth metal) .

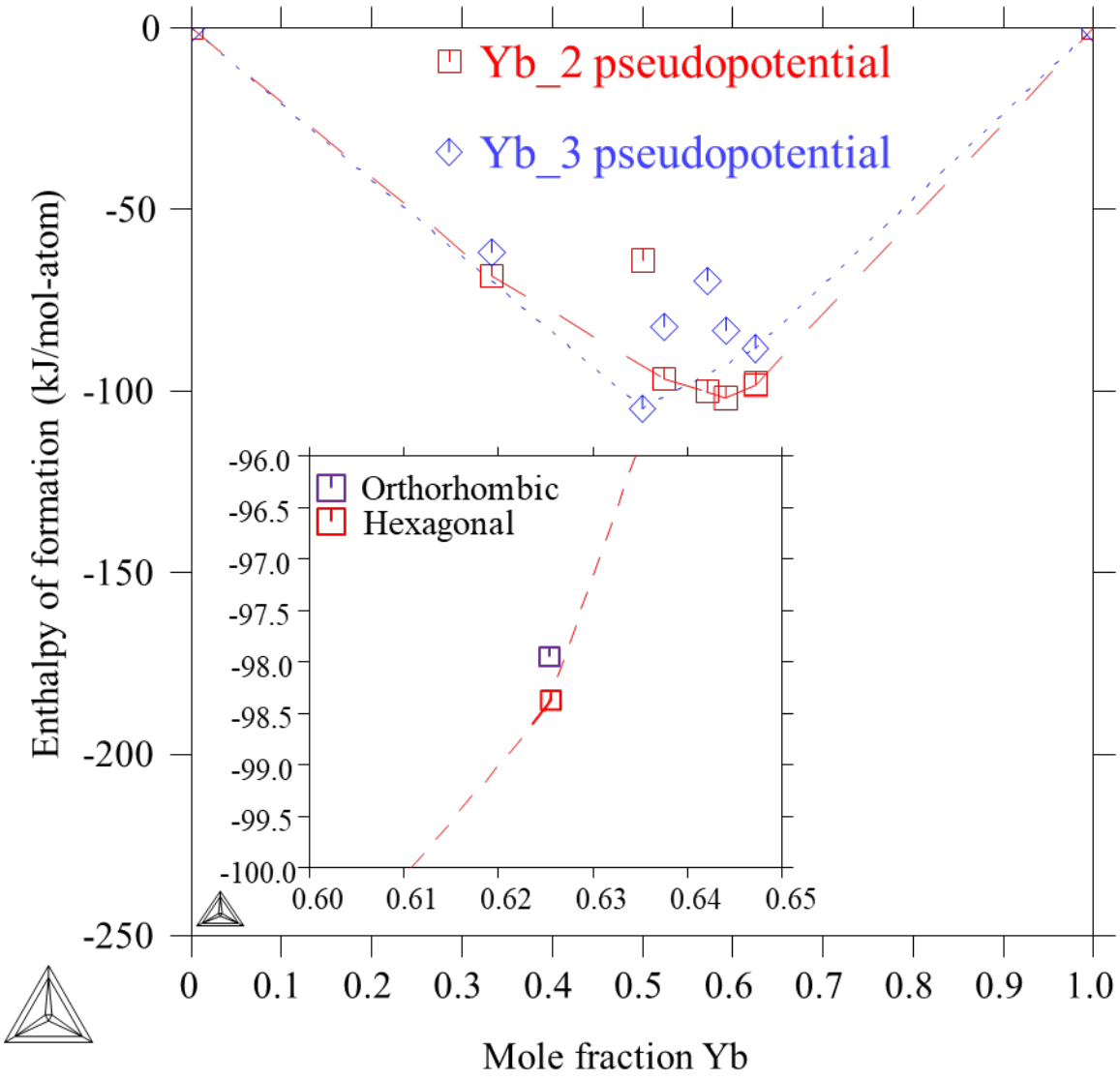

Figure 2 Enthalpies of formation of intermetallic compounds in the Yb-Sb system predicted by DFT at 0 K applying both Yb_2 (□) and Yb_3 (◇) pseudopotentials from Chong et al.'s work [19]. Zoomed in image shows the enthalpies of formation of orthorhombic and hexagonal Yb_5Sb_3 predicted with Yb_2 and their relation to the convex hull.

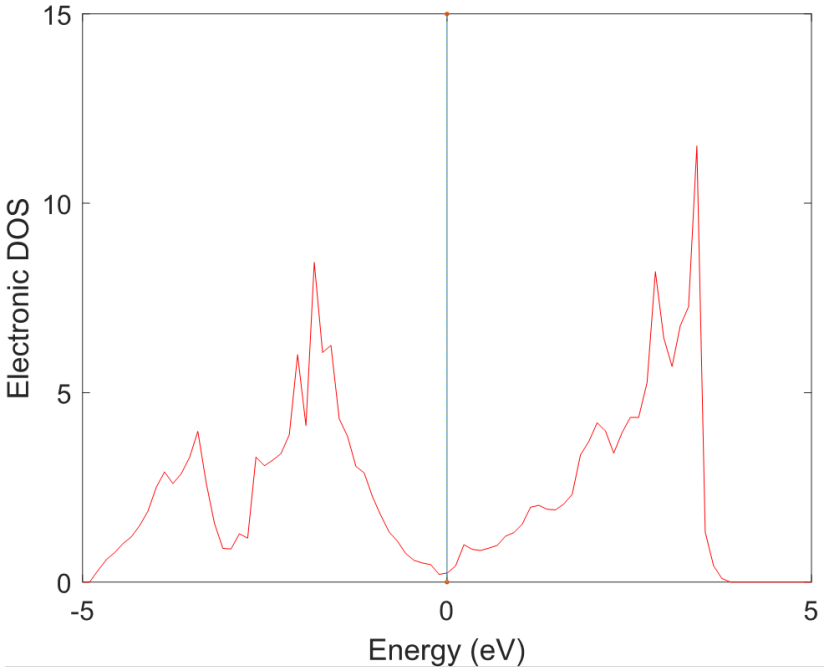

Figure 3 Electronic density of states of the rocksalt YbSb compound predicted by first-principles calculations based on DFT with the Yb_3 pseudopotential. The energies are referenced to the Fermi energy (blue line).

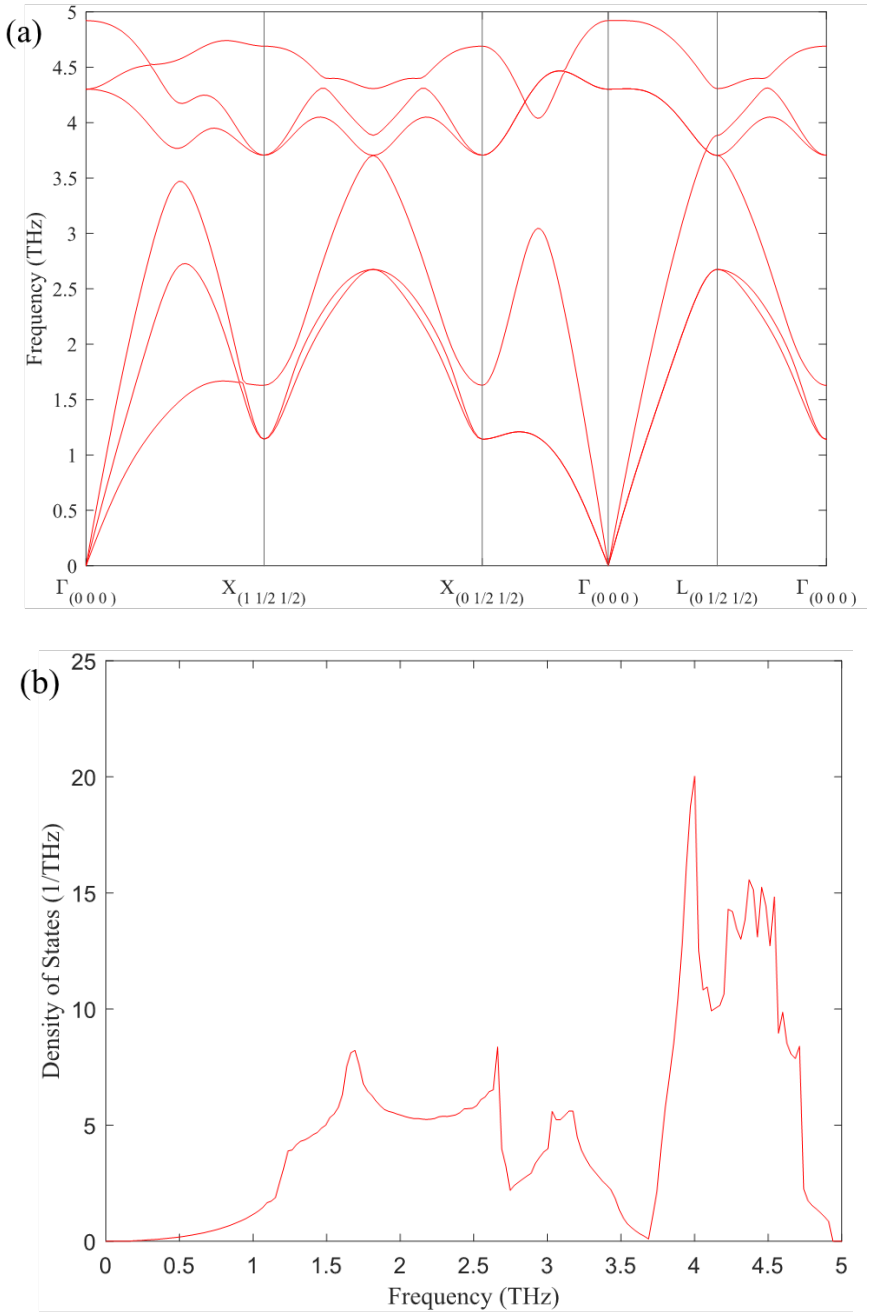

Figure 4 (a) Phonon dispersion of the YbSb phase in the rocksalt structure plotted along the presented symmetrical principal directions. (b) Total phonon density-of-states as a function of frequency (THz).

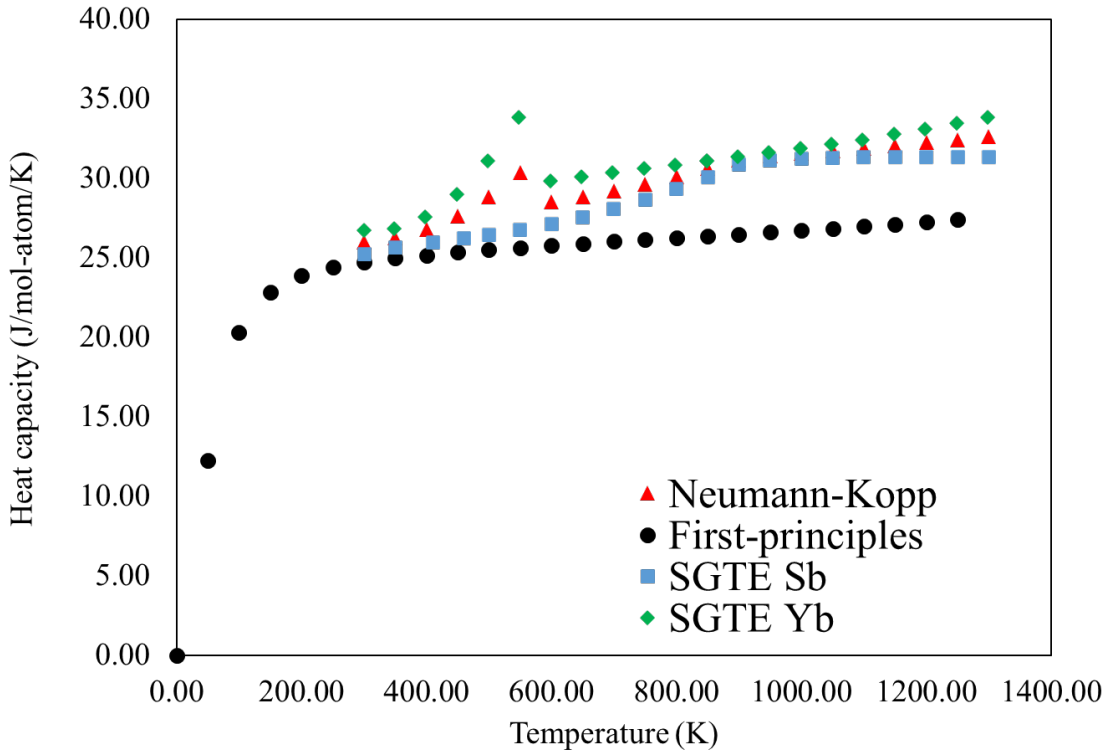

Figure 5 Heat capacity as a function of temperature of the YbSb compound predicted by the Neumann-Kopp approximation (▲) and phonon supercell calculations (●) alongside the heat capacity from the SGTE database of FCC Yb (◆) and Rhombohedral Sb (■) for comparison.

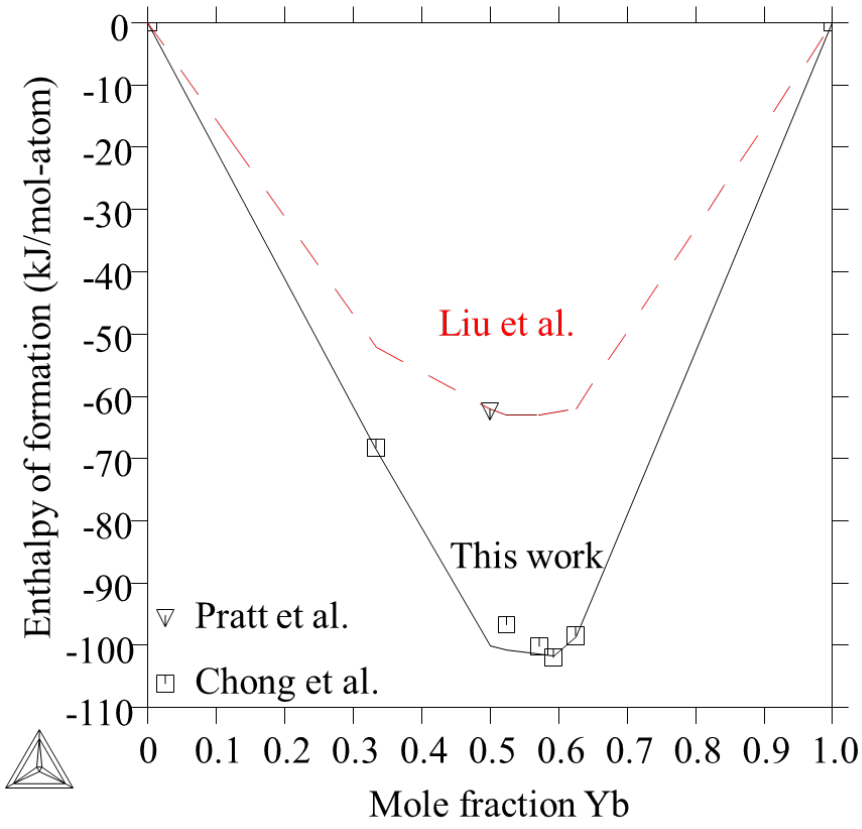

Figure 6 Enthalpies of formation at 300 K of the intermetallic compounds in the Yb-Sb system, with the dashed and solid curves representing Liu et al.'s [15] and this study's CALPHAD modeling, respectively. The square symbols (□) represent the DFT-based calculations using Yb_2 pseudopotential [19] and the triangle (▽) represents experimental value measured by Pratt et al.[14].

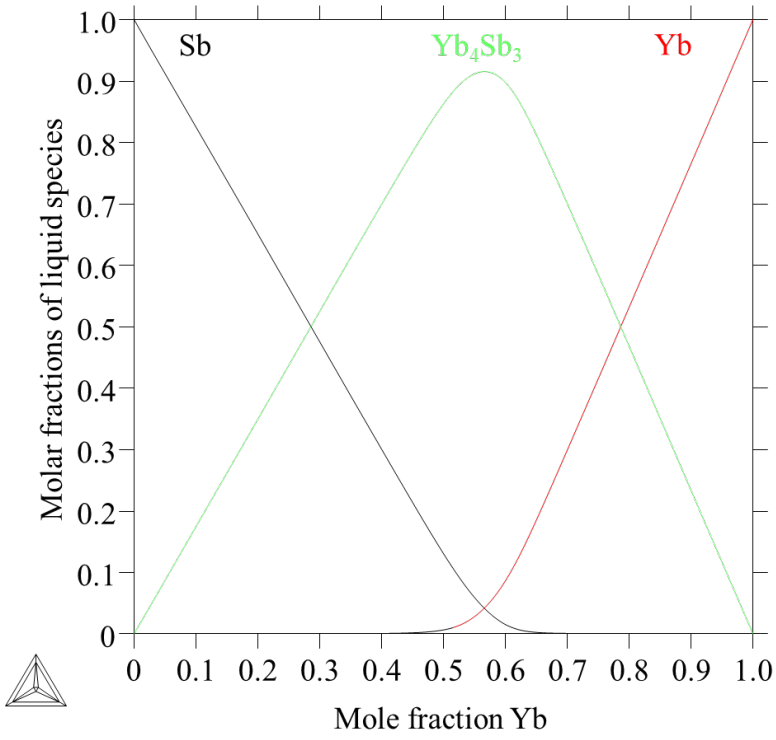

Figure 7 Mole fraction of species in the liquid phase as a function of mole fraction of Yb at 1973 K from the present study's CALPHAD modeling.

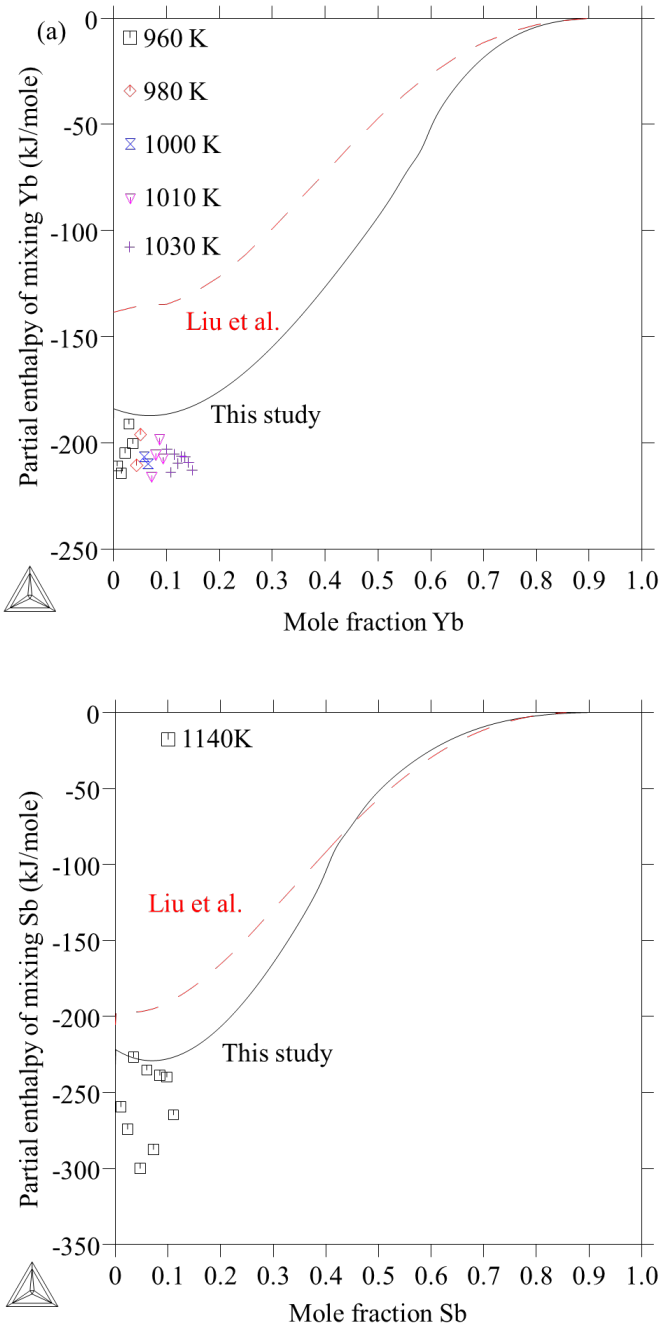

Figure 8 (a) Partial enthalpy of mixing of Yb at 1030 K and (b) Sb in liquid at 1140 K of both Liu et al.'s [15] and the present work's models compared with experimental data from Sudavtsova et al. [28] at multiple temperatures.

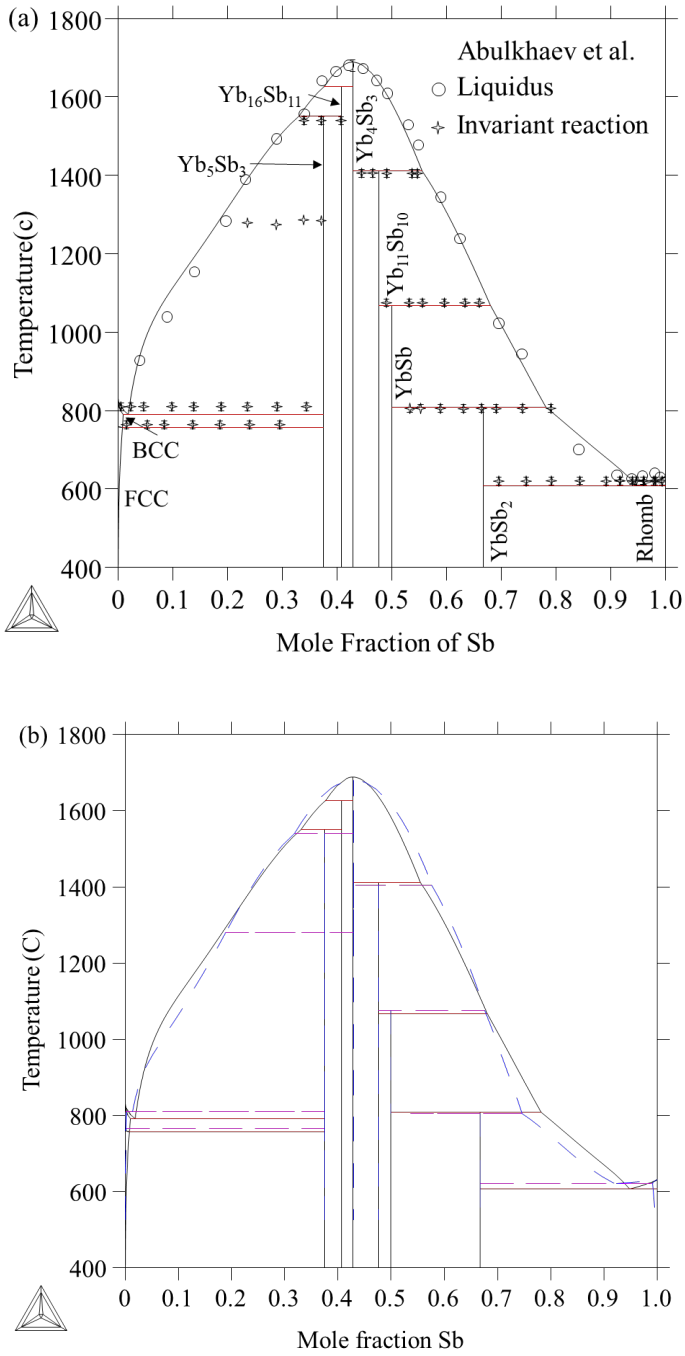

Figure 9 (a) Calculated phase diagram of the Yb-Sb system in the present study compared with experimental data [13] (b) Calculated phase diagram of this study and Liu et al.'s [15] work (Blue and pink dashed lines).

7

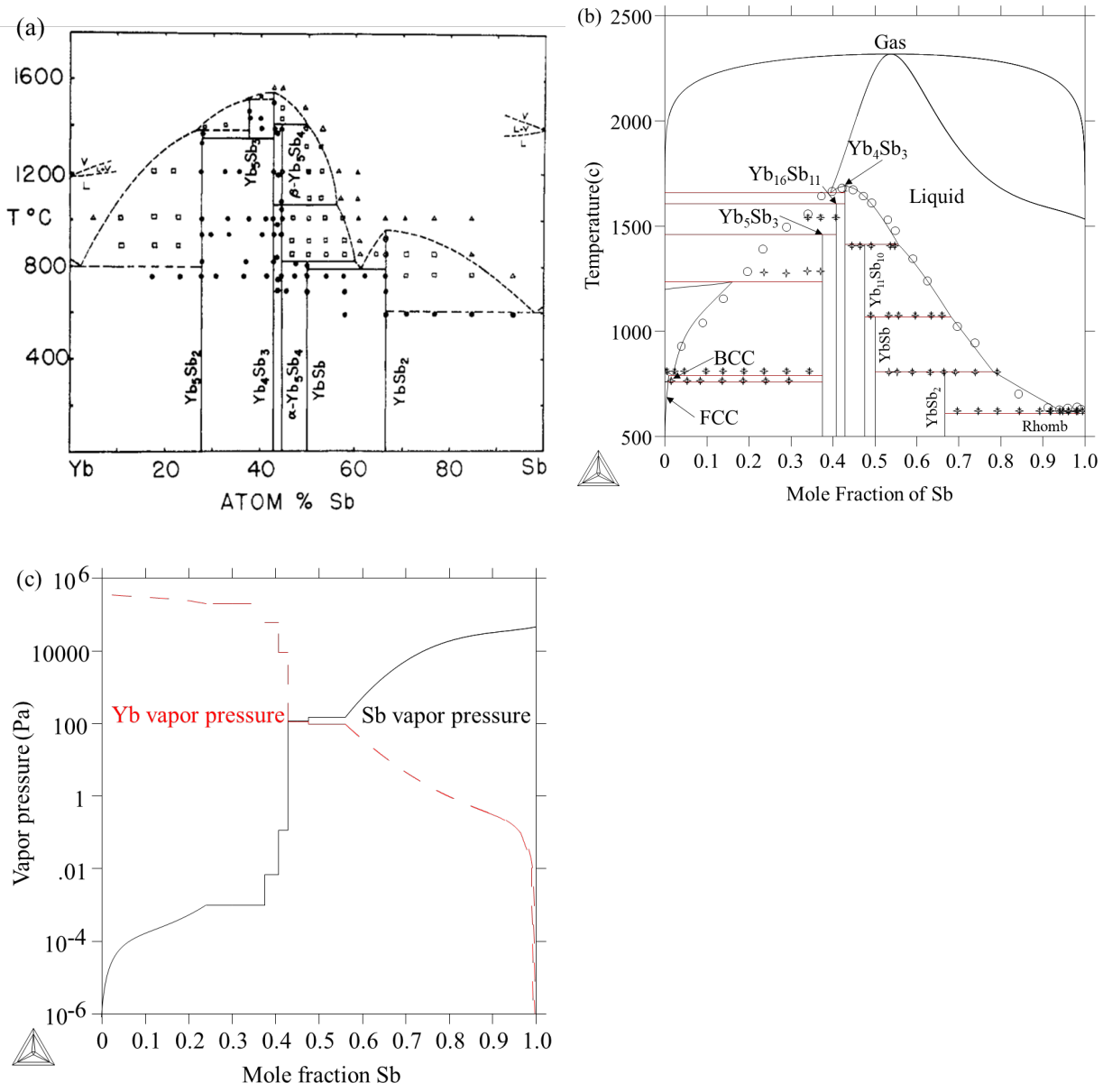

Figure 10 (a) Proposed phase diagram by Bodnar et al. [25]: (○) single-phase solid region; (●) two-phase solid region; (△) liquid; (□) liquid and solid (b) Calculated phase diagram including the gas phase modeled in the SGTE database at the total pressure of 101325 Pa. (c) Partial vapor pressures of Yb and Sb at 1673 K as a function of composition.